Available online at www.sciencedirect.com
ScienceDirect
Trans. Nonferrous Met. Soc. China 31(2021) 1339−1349
Transactions of Nonferrous Metals Society of China
www.tnmsc.cn

Microstructure and mechanical properties of Ti−6Al−4V/Ti−22Al−25Nb joint formed by diffusion bonding

Peng LIN[1,2], Xian-zheng XI[1], Wen-kai ZHAO[1], Rui-hongYANG[1], Fei LIN[1], Xiao-lei CUI[2], Gang LIU[2]

1. College of Materials Science and Engineering, Taiyuan University of Technology, Taiyuan 030024, China;
2. State Key Laboratory of Advanced Welding and Joining, Harbin Institute of Technology, Harbin 150001, China

Received 20 May 2020; accepted 24 January 2021

Abstract: Ti−6Al−4V (wt.%) and Ti−22Al−25Nb (at.%) were joined by diffusion bonding at 950 °C and 15 MPa for 100 min, and the microstructure and mechanical properties of the resulting joints were investigated. The composition of the diffusion layer is *B*2/discontinuous α/α_2 layer/necklace-shaped $\beta+\alpha'$ layer, where the content of any element at a given point mainly depends on the distance of the point from the interface and the phase type at the point. The tensile strength of the joint is 894 MPa, which is almost the same as that of the Ti−22Al−25Nb base alloy. The fracture surfaces on both sides of the joint are composed of two main regions. One region displays a relatively flat surface and fractures along the bonding interface. The other is composed of a moderate number of irregularly-shaped cavities on the Ti−6Al−4V side and many irregularly-shaped bulges on the Ti−22Al−25Nb side. Both regions result from fracture along the boundaries between $\beta+\alpha'$ layers and α_p grains or from the transcrystalline fracture of α_p grains.
Key words: diffusion bonding; Ti−6Al−4V; Ti−22Al−25Nb; interface; diffusion layer

1 Introduction

Due to their low weight, high strength, low thermal expansion, and excellent creep/corrosion resistance, titanium alloys, such as Ti−6Al−4V, have been widely used in the aerospace industry. WRONSKI et al [1] proposed the use of titanium alloys in the static and rotating components of turbine engines, but NARAYANA et al [2] thought that the stability of their structures is restricted by the temperature at which the α phase transforms into the β phase (882 °C for pure titanium); thus, such alloys have a temperature limit of 550−600 °C. In contrast, NANDY and BANERJEE [3] claimed that the orthorhombic titanium aluminides based on the intermetallic compound of Ti_2AlNb (*O*-phase) can be used in applications at elevated temperatures (600−700 °C) due to their high tensile and fatigue strengths, good creep and oxidation resistance, and low coefficient of thermal expansion. The unit cell of Ti_2AlNb is orthorhombic, the point group is *mmm,* and the space group is *Cmcm*. The orthorhombic crystal structure of Ti_2AlNb can be considered as a mixture of hexagonal D019 Ti_3Al (α_2-phase) and a bcc *B*2 ordered titanium solid solution [4]. KUNPFERT [5] believed that this new class of alloys can compete with conventional near-α titanium alloys, the most mature gamma Ti−Al alloys, and even nickel-based materials; however, Ti_2AlNb base alloys have shown some disadvantages such as a higher density (5.3 g/cm^3), worse workability, and higher production costs than conventional titanium alloys. Therefore, it is still more advisable to use conventional titanium alloys at positions where the working temperature is below 600 °C. In practical applications where a temperature gradient is involved, it may be necessary to join two different materials to produce dual-property components.

Corresponding author: Peng LIN, Tel: +86-351-6010021, E-mail: linpeng@tyut.edu.cn; Gang LIU, E-mail: gliu@hit.edu.cn
DOI: 10.1016/S1003-6326(21)65581-4

Diffusion bonding produces solid-state coalescence between two materials by applying pressure at a temperature below the melting point of the materials to be joined [6,7]. ELREFAEY and TILLMANN [8] found that this technique avoids many of the problems encountered during fusion welding, such as cracking, and produces joints with minimum macroscopic deformation without deteriorating the mechanical properties of the base metals; thus, it is a near-net-shape forming process for joining dissimilar materials. The diffusion bonding of Ti-alloys and dissimilar γ-TiAl/Ti alloys has been investigated [9−16]. HOLMQUIST et al [17] studied the hot isostatic diffusion bonding of Ti−6Al−4V/γ-TiAl IHI 01A alloys under the condition of 900−980 °C, 45 MPa and 2 h and found that the diffusion bondline showed two zones, and the ultimate tensile strength reached 420−480 MPa. HOLMQUIST et al [18] also investigated the tensile and creep properties of IMI 384 titanium alloy to IHI 01A γ-TiAl joint, and the resulting ultimate tensile strength was slightly lower than that of the γ-TiAl base alloy at all examined temperatures except 600 °C, indicating that sound joints with good mechanical properties can be achieved by diffusion bonding. WANG et al [19] fabricated sound Ti−43Al−9V/Ti−6Al−4V joints using vacuum hot-pressing under the condition of 920 °C, 45 MPa and 2 h and found that the interfacial phase sequence of the as-prepared joints was Ti−43Al−9V/γ-TiAl/$B2$/α_2-Ti_3Al/α-Ti/Ti−6Al−4V, indicating that the preferred reaction phase between TiAl intermetallics to Ti alloys was an α_2-Ti_3Al phase. LI et al [20] used hot-press bonding between Ti−33Al−3V and TC17 at 850 °C and different pressures for 10 min and obtained a maximum bonding ratio of 96.3% at a pressure of 50 MPa with post-bonding heat treatment. XUE et al [21] utilized single Ti-based amorphous or Ni-based amorphous foils as an interlayer for the diffusion bonding of metallurgical powder TiAl-based alloy and Ti−6Al−4V alloy at 915 °C and 80 MPa for 1 h. They concluded that adding Ti-based amorphous interlayer improved atomic diffusion, which ultimately improved the mechanical properties of the joints.

The above previous literatures demonstrate the possibility of joining γ-TiAl to Ti alloys by diffusion bonding; however, few literatures have reported the diffusion bonding between Ti_2AlNb (or Ti_3Al) base alloys and conventional titanium alloys. Due to different compositions, microstructures, and mechanical properties of TiAl and Ti_2AlNb base alloys, the suitable process parameters, such as the bonding temperature, pressure, and holding time will be different. The joint characteristics, including the interface microstructure and mechanical properties, will also be different.

In this study, the diffusion bonding of Ti_2AlNb base alloy (Ti−22Al−25Nb) to Ti−6Al−4V at 950 °C under an applied pressure of 15 MPa for 100 min was investigated. The interfacial microstructure and elemental distribution were analyzed, and the mechanical properties of the joints were tested. The underlying relationship between the mechanical properties and the microstructure in the base materials, as well as in the bondline, was determined. Fractographic studies were also performed to elucidate the role of the interfacial microstructure in the fracture process. This work may help to develop dual-property components based on Ti_2AlNb/Ti.

2 Experimental

Cylindrical blanks with dimensions of d20 mm × 25 mm were cut from an extruded Ti−6Al−4V alloy bar and a forged Ti−22Al−25Nb (at.%) disk with flat end surfaces perpendicular to the axis of the bar or the disk for diffusion bonding. The mating surfaces of all blanks were ground using silicon carbide waterproof sandpapers down to grit 2000# and cleaned using an ultrasonic cleaning machine. Figure 1 shows a schematic illustration of the diffusion bonding process, which was carried out through hot-pressing at 950 °C and 15 MPa for 100 min on a hydraulic machine attached with a high-temperature furnace. The microhardness of the bonding interface and base materials was measured with a Vickers microhardness tester under an indentation load of 25 g for 5 s. The microhardness was evaluated by taking five indentations, and only the middle three values were averaged. The tensile samples with a gauge size of 10 mm (length) × 3 mm (width) × 2 mm (thickness) were prepared, ensuring that the gauge length direction was perpendicular to the bonding interface. Three tensile samples were prepared for each joint. The tensile tests were done at room temperature and a strain rate of 1×10^{-3} s^{-1}

on a testing machine. The samples for microstructure observations were prepared by electrochemical polishing in a solution of 6% perchloric acid, 34% butanol, and 60% carbinol at −40 °C. The interfacial microstructure and elemental distribution were analyzed with a field emission scanning electron microscope equipped with an energy-dispersive spectrometer.

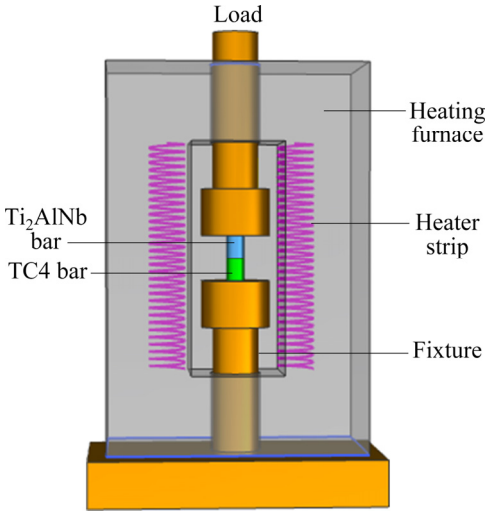

Fig. 1 Schematic illustration of diffusion bonding between Ti_2AlNb and Ti−6Al−4V

3 Results and discussion

The microstructures of the as-received Ti−6Al−4V bar and Ti−22Al−25Nb disk are shown in Figs. 2(a) and 2(b), respectively. The Ti−6Al−4V alloy consists of two phases: nearly fully-equiaxed α-phase grains with a size of 20−50 μm and intergranular β-phase layers around the α-phase grains. The Ti−22Al−25Nb alloy consists of three phases: a continuous $B2$ phase matrix, equiaxed α_2-phase particles, and acicular O-phase laths, which appear as bright, dark, and gray in contrast, respectively.

Figure 3 shows the SEM micrographs of the as-prepared joints. After holding at 950 °C for 100 min, the microstructure of the two base alloys is changed. In the Ti−22Al−25Nb base alloy, some acicular O-phase laths, especially the smaller ones, are partially dissolved in the $B2$ matrix. In the Ti−6Al−4V base alloy, the initial intergranular β layers among α grains coarsen into irregularly-shaped blocks. The secondary α-phase (α_s) precipitates in the β blocks during cooling from the diffusion bonding temperature to room temperature,

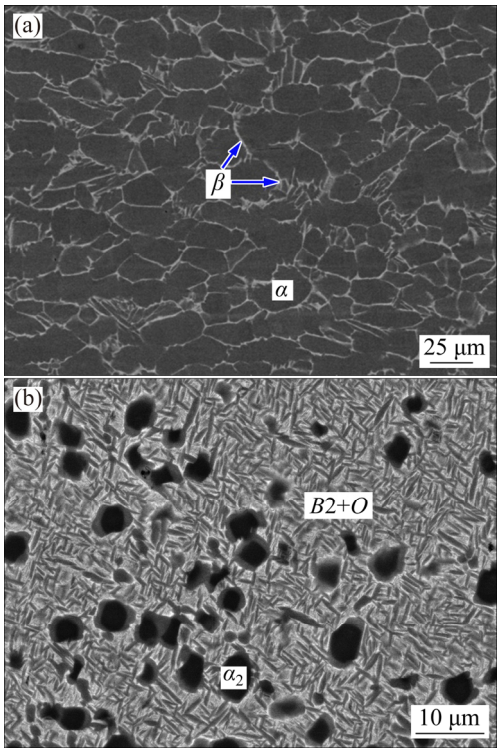

Fig. 2 Backscattered electron (BSE) SEM images showing microstructure of two base alloys in annealed condition: (a) Ti−6Al−4V alloy; (b) Ti−22Al−25Nb alloy

which leads to the formation of $\beta+\alpha_s$ colony-type microstructure, as shown in Fig. 3(c). Accordingly, the whole microstructure is transformed into a bimodal (duplex) microstructure containing equiaxed primary α (α_p) phase in lamellar $\beta+\alpha_s$ matrix. This is the most widely-used microstructure as it possesses the best combination of strength, ductility, and fatigue properties [22,23]. The interface between the two bonded alloys is marked with black lines in Fig. 3. There are no obvious defects, such as voids or gaps on or near the interface, indicating good bonding between the two alloys under the condition of 950 °C, 15 MPa and 100 min.

Due to element interdiffusion between the two alloys, the microstructure morphology on both sides of the interface significantly changes compared with that in both base materials. On the Ti−22Al−25Nb side, the easily distinguished boundary between the diffusion layer and base material is smooth and about 15 μm in width. In contrast, on Ti−6Al−4V side, no evident boundary was detected. The diffusion layer can be divided into two sub-layers. Next to the interface is a discontinuous layer, which is shown as the dark

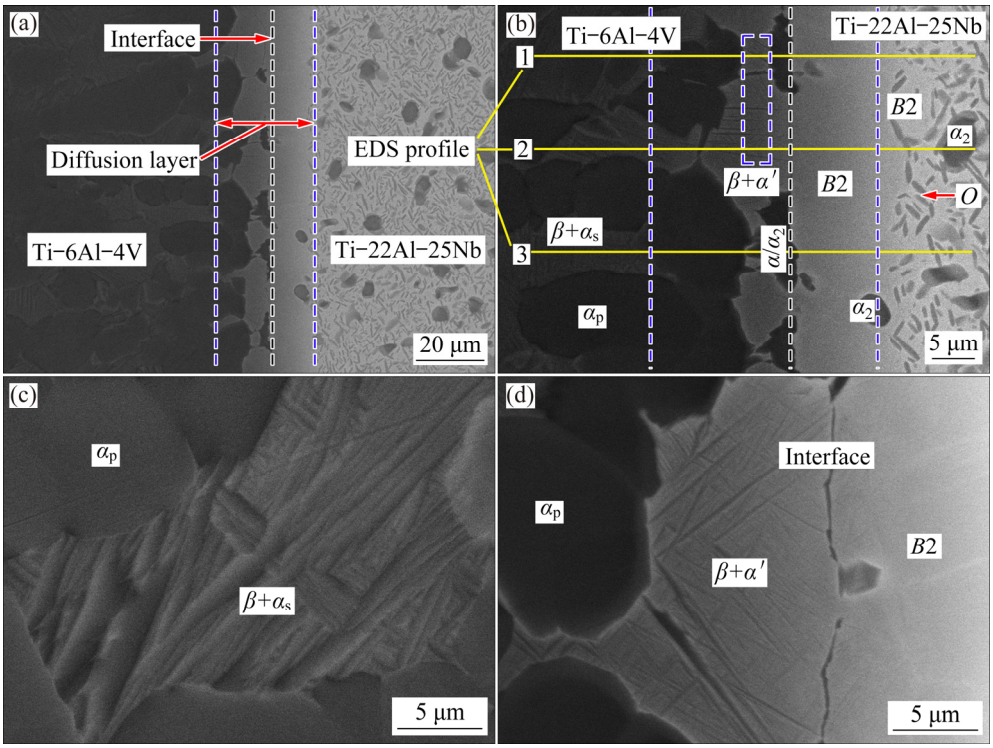

Fig. 3 BSE-SEM images of diffusion-bonded joints between Ti−22Al−25Nb and Ti−6Al−4V alloys bonded at 950 °C and 15 MPa for 100 min: (a) Low-magnification image; (b) High-magnification image; (c) $\beta+\alpha_s$ colony microstructure in Ti−6Al−4V base alloy; (d) $\beta+\alpha'$ martensitic microstructure in diffusion layer

α_p-phase. The maximum Al content in this layer is 22.6 at.% or 13.2 wt.%, which is much higher than its maximum solubility (about 7 wt.%) in titanium at room temperature. Therefore, the phase composition of this layer should be a mixture of α and α_2 phases. ZAFARI and XIA [24] proposed that there is an almost continuous necklace-shaped layer between the interface and Ti−6Al−4V base alloy, which is not a colony microstructure but a martensitic structure, that is, more refined acicular martensitic α'-phase laths precipitate in β matrix.

EDS maps describing the qualitative elemental distribution in the joint are shown in Fig. 4. The number of dots in each map indicates the presence of a certain element, which is related to its concentration. EISENBARTH et al [25] stated that since Al is α-phase stabilizer, and V and Nb are β-phase stabilizers, the α and α_2 phases are rich in Al, while the β and $B2$ phases are rich in V and Nb. As a result, in the diffusion layer, more Nb atoms diffuse from Ti−22Al−25Nb side into the β-phase than into the α-phase on Ti−6Al−4V side, causing the β-phase adjacent to the interface to show a lighter contrast and grow into large blocks. ELIAS et al [26] noted that this is also due to the stabilizing effect of Nb on the β-phase, which causes the CCT diagram to shift to the right of the martensitic transformation line (M_s), leading to the precipitation of acicular martensite α'-phase in the β-phase adjacent to the interface. In contrast, more Al atoms diffuse from Ti−22Al−25Nb side into the α_p-phase on Ti−6Al−4V side because Al stabilizes the α-phase. A few β-phase stabilizer V atoms on Ti−6Al−4V side also diffuse into the $B2$ phase on Ti−22Al−25Nb side.

Figure 5 shows the content profiles of elements across the diffusion layer, where the diffusion layer is only composed of $B2$ and $\beta+\alpha'$ regions, such as Profile 2 shown in Fig. 3(b). The content gradient of the four elements is nearly continuous. However, when the content profile passes different phases, such as Profiles 1 and 3, the content gradient shows a sharp jump. The diffusion flux of Nb and Al atoms are from Ti−22Al−25Nb towards Ti−6Al−4V, while V and Ti atoms diffuse in the opposite direction, that is, the four elements all diffuse from a high content to a low concentration, which is termed downhill diffusion. The EDS line scanning results show that the total width of the diffusion layer is about 40 μm: 15 μm

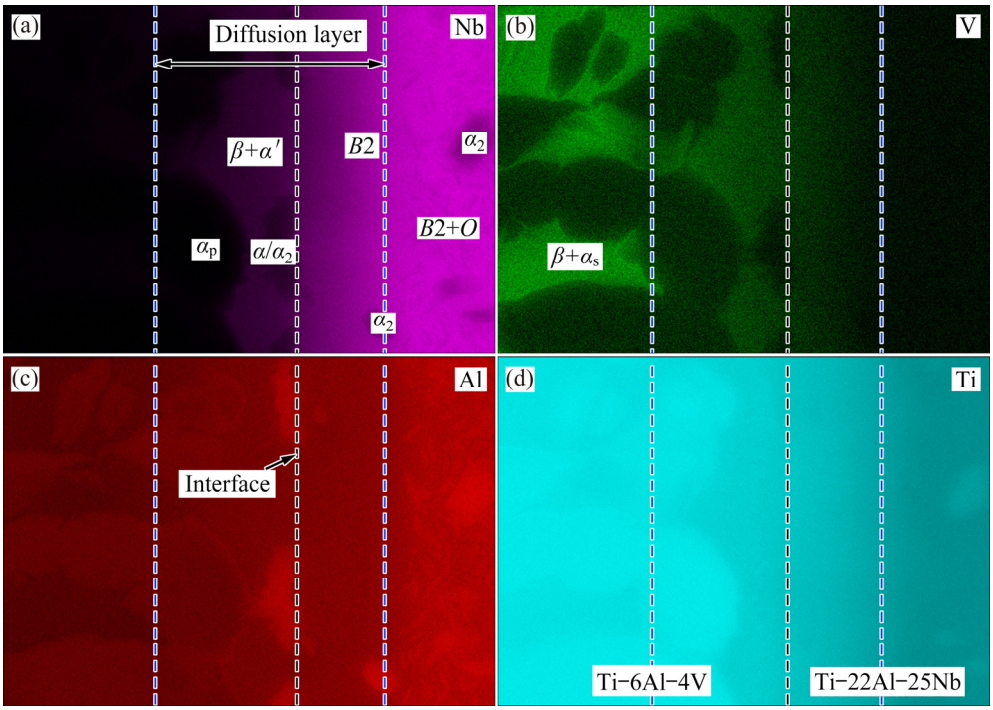

Fig. 4 EDS map of joint shown in Fig. 3(b) and distributions of Nb (a), V (b), Al (c) and Ti (d) elements

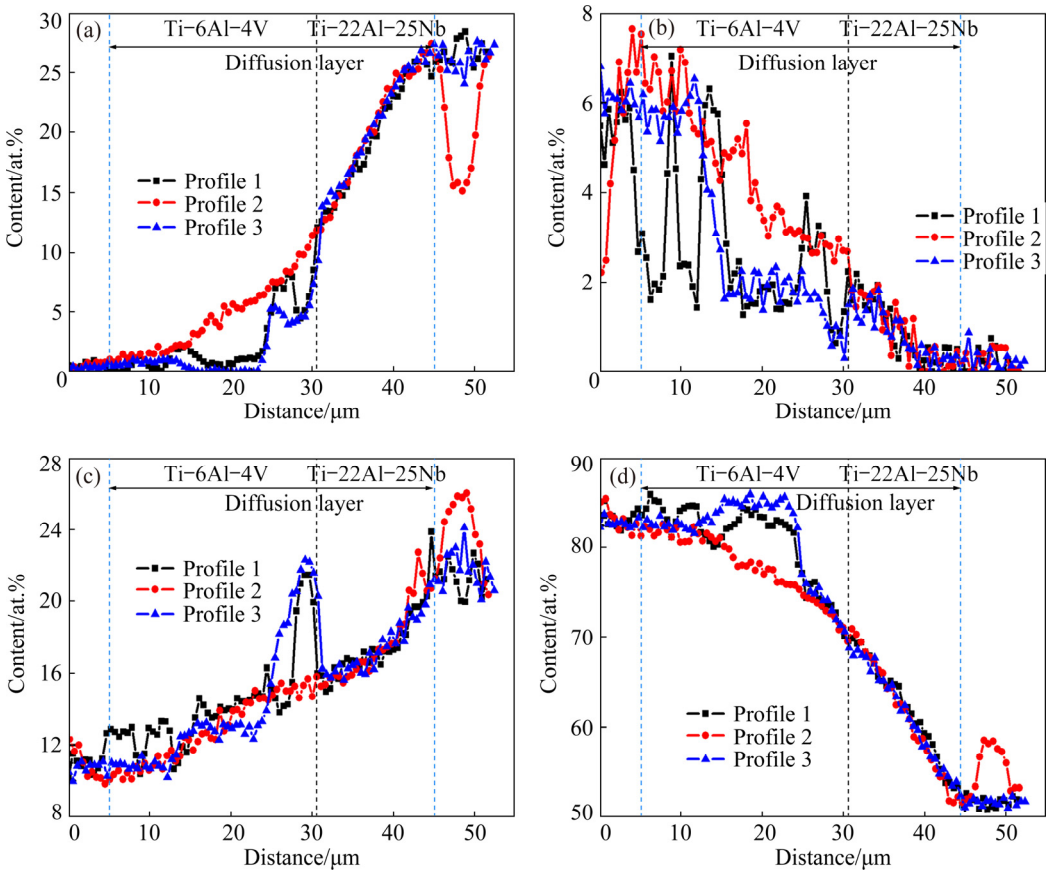

Fig. 5 Content profiles of Nb (a), V (b), Al (c) and Ti (d) elements across diffusion layers

on Ti−22Al−25Nb side and 25 μm on Ti−6Al−4V side. The content of any element at a certain point mainly depends on the distance of this point from the interface and the phase type where the point is located; therefore, the content curves along the three profiles in the same phase region overlap. It is

noteworthy that the Nb content curves in Profiles 1 and 2 within the x-coordinate scale from 25 to 27 μm (marked with a rectangle in Fig. 3(b)) also overlap, although the $\beta+\alpha'$ layer is isolated, and the transverse diffusion flux is hindered by the α/α_2 layer in Profile 1. This indicates that diffusion occurs not only in the transverse direction but also in the longitudinal direction. The atomic radii of Ti, Al, Nb and V are 0.145, 0.143, 0.143 and 0.135 nm, respectively, implying that the vacancy mechanism is the main diffusion mechanism during the whole diffusion bonding process.

The Vickers microhardness values of the bonding interface zone and the two base alloys are measured, as shown in Fig. 6. For the Ti−6Al−4V base alloy, the microhardness values of the primary α_p grain and the $\beta+\alpha_s$ colony regions are HV 347 and HV 308, respectively. The former is larger than the latter because the α-phase generally has a higher strength than the β-phase. YAN et al [27] measured the nanohardness values of primary α_p grains and transformed $\beta+\alpha_s$ colony structure by nanoindentation mapping a series of bimodal microstructures with different volume fractions of primary α_p grains. The results also showed that the primary α_p grains are harder than the transformed $\beta+\alpha_s$ colony structure. In addition, the hardness difference between the two components gradually decreases upon increasing the intercritical annealing temperature (i.e., increasing the volume fraction of transformed $\beta+\alpha_s$ colony regions) and nanohardness. Its evolution with annealing temperature is dominated by the solution hardening of α-phase by Al. However, this result is contradicted by the commonly-held notion that the transformed $\beta+\alpha_s$ area is harder than the primary α_p grains due to the precipitation of fine secondary α_s plates. In contrast, the hardness of the $\beta+\alpha'$ martensitic structure in the diffusion layer on the Ti−6Al−4V side is HV 385, which is the hardest region in the whole joint sample. For this reason, LÜTJERING [28] pointed out that the acicular martensitic α'-phase has a much greater strengthening effect on the β matrix than the secondary α_s plates, but the diffusion of Al and Nb atoms into the layer enhances the solution strengthening effect. These double strengthening mechanisms result in the high tensile strength of the joints. In contrast, the hardness of the $B2$ layer on the Ti−22Al−25Nb side decreases from HV 324 to HV 309 in the Ti−22Al−25Nb base alloy because some Al and Nb atoms diffuse out from this layer, which weakens the solution strengthening effect. The dissolution of O-phase precipitates also weakens the precipitation strengthening effect.

The tensile properties of the as-received base materials are shown in Fig. 7(a), and the tensile

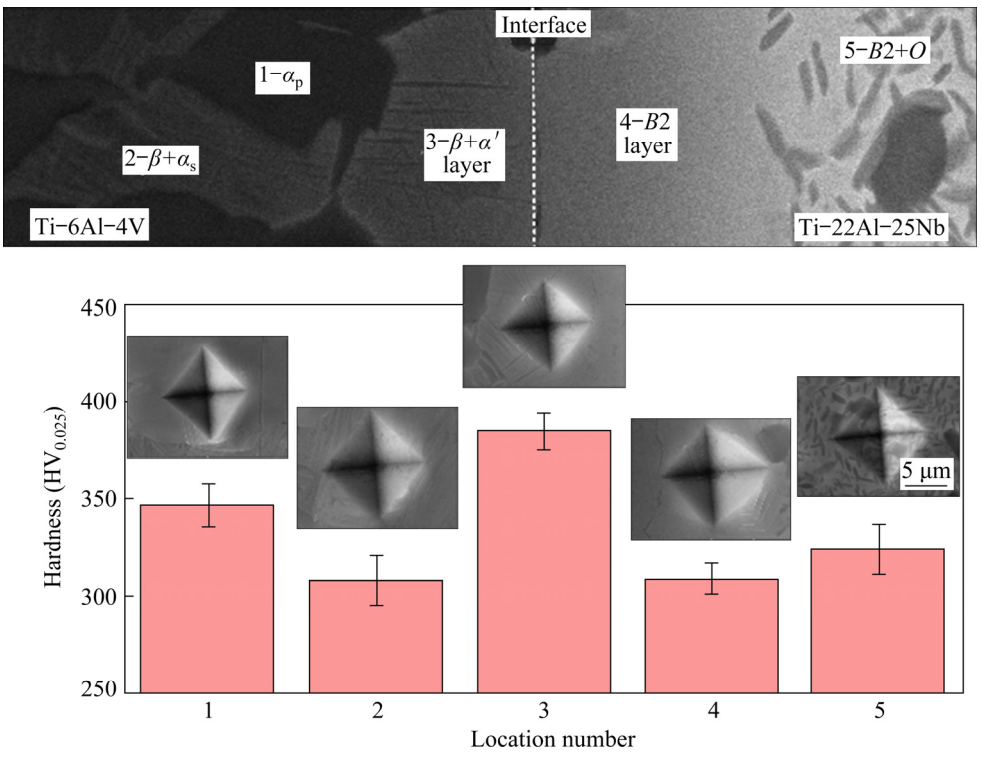

Fig. 6 Microhardness of bonded joints

properties of the joint and the base materials after diffusion bonding are shown in Fig. 7(b). The yield strength (YS) and ultimate tensile strength (UTS) of the as-received Ti−6Al−4V are 740 and 815 MPa, respectively; however, after annealing at 950 °C for 100 min during diffusion bonding, the YS and UTS increase to 818 and 936 MPa, respectively, while the elongation to failure drops from 18% to 14%. Although the transformed $\beta+\alpha_s$ colony microstructure has a lower hardness than the primary α_p-phase, it increases the YS and UTS of the whole sample. YAN et al [27] also found that the tensile strength of Ti−6Al−4V alloy increases upon increasing the volume fraction of transformed $\beta+\alpha_s$ colony microstructure. JUN et al [29] concluded that dislocation glide inside the primary α_p grains is blocked at the interfaces between the primary α_p grains and transformed $\beta+\alpha_s$ regions. The transformed $\beta+\alpha_s$ regions have finer microstructures, and more phase or grain boundaries mainly serve to strengthen the tensile properties of the bimodal microstructures. The YS and UTS of the as-received Ti−22Al−25Nb samples are 800 and 990 MPa, respectively; however, they decrease to 732 and 891 MPa, respectively, after annealing, while the elongation to failure increases from 4.5% to 14%. This indicates that the dissolution of *O*-phase laths, especially those with small sizes, into the *B*2 phase matrix helps improve the ductility, but the strength is decreased. This follows the traditional precipitation strengthening mechanism, as reported by BOEHLERT [30]. The tensile stress−strain curves of the joint and Ti−22Al−25Nb base alloy show significant overlap, indicating that deformation mainly occurs on the Ti−22Al−25Nb side due to its lower YS than that of Ti−6Al−4V. The strength of the joint approaches 894 MPa, which is almost equal to that of the Ti−22Al−25Nb base alloy.

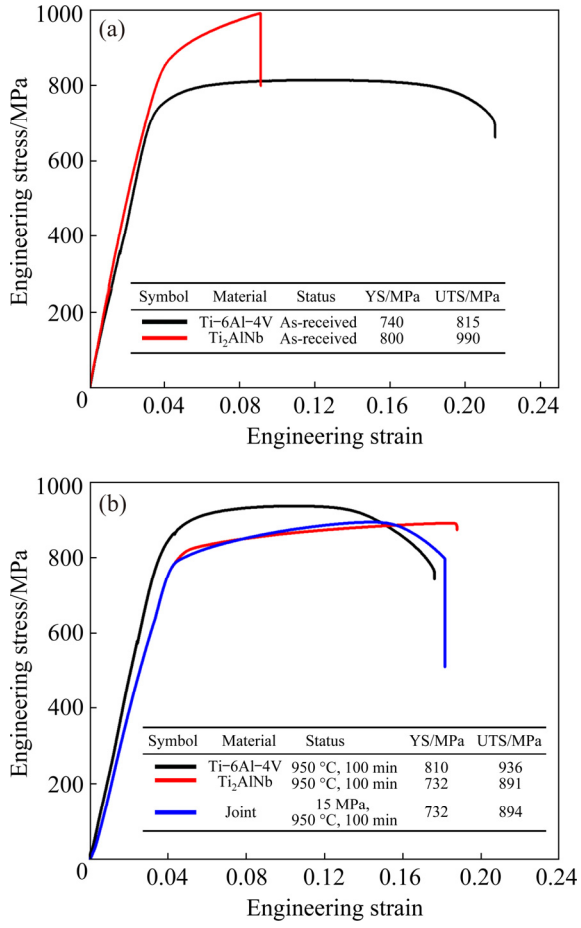

Fig. 7 Tensile properties of as-received base materials (a) and joint and base materials after diffusion bonding at 950 °C and 15 MPa for 100 min (b)

Figure 8 shows the surface morphology of the fractured joint. The fracture location is mainly concentrated in two regions. One is along the bonding interface between the two base alloys, where the $\beta+\alpha'$ layer is generally much thinner, as indicated by "I" in Fig. 8. The other is along the boundaries between the $\beta+\alpha'$ layer and the initial primary α_p grains on the Ti−6Al−4V side, where the $\beta+\alpha'$ layer is generally thicker, as indicated by "II" in Fig. 8. The fracture profile in Region II appears wavy due to the necklace shape in the $\beta+\alpha'$ layer. As shown in Fig. 9(b), in some regions where the fracture occurs along the bonding interface, the α/α_2 layer is attached to the $\beta+\alpha'$ layer, indicating that

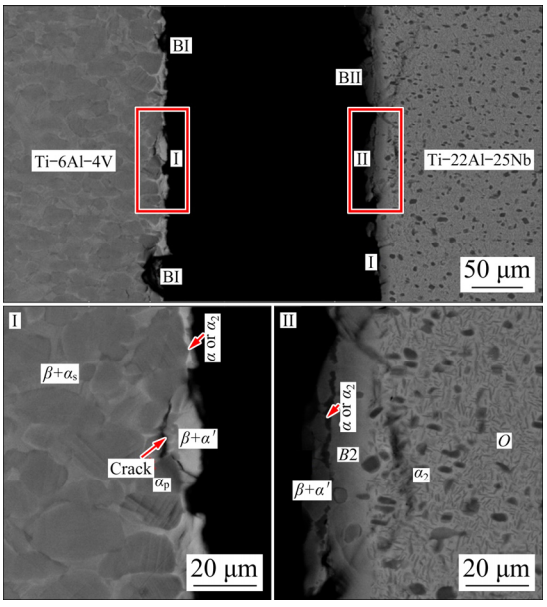

Fig. 8 Surface morphologies of fractured joint bonded under condition of 950 °C, 15 MPa and 100 min

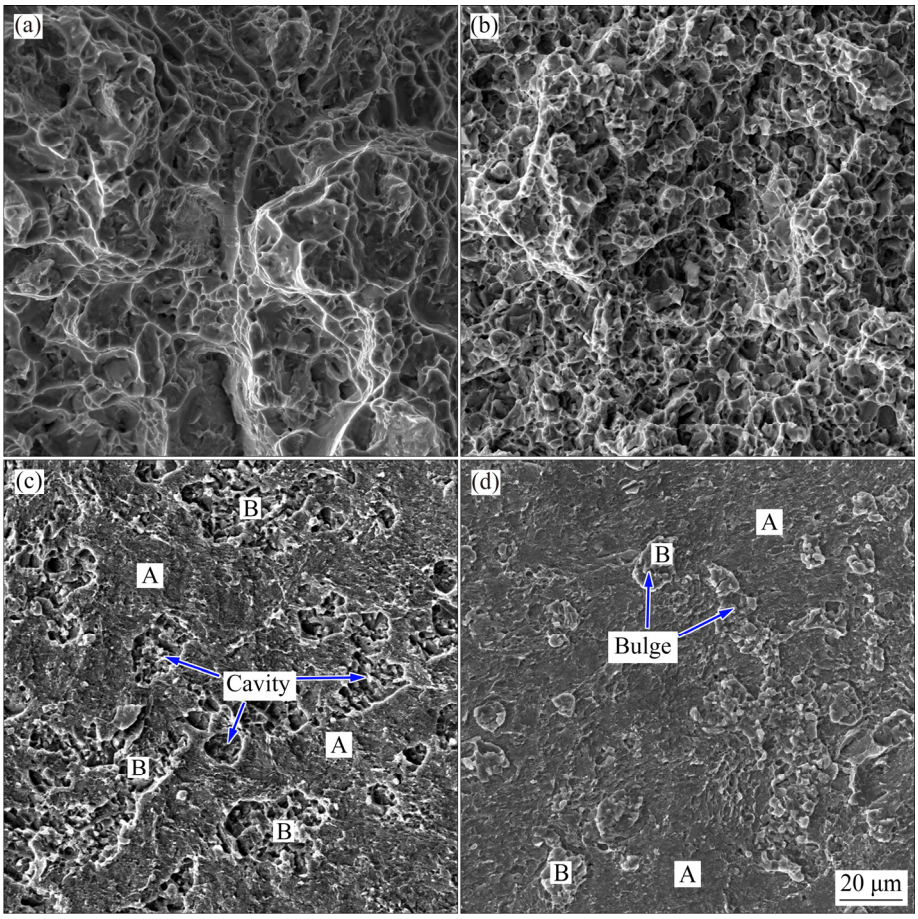

Fig. 9 Tensile fracture morphologies of Ti−6Al−4V base alloy (a), Ti−22Al−25Nb base alloy (b), Ti−6Al−4V side of joint (c) and Ti−22Al−25Nb side of joint (d) after diffusion bonding under condition of 950 °C, 15 MPa and 100 min

the bond strength of the α/α_2 layer to the $\beta+\alpha'$ layer is greater than that to the *B*2 layer on the Ti−22Al−25Nb side. This is because the α/α_2 layers originally belong to the primary α_p grains on the Ti−6Al−4V side and are not thoroughly isolated by the thinner $\beta+\alpha'$ layers. In contrast, in Region II, the diffusion layer on the Ti−6Al−4V side, including the α/α_2 layer and the $\beta+\alpha'$ layer, is completely attached to the *B*2 layer on the Ti−22Al−25Nb side, indicating that the bond strength of the interface between the two base alloys is greater larger than that between the thick $\beta+\alpha'$ layer and the initial α_p grains on the Ti−6Al−4V side. Therefore, the weakest region in the whole joint sample is located at the interface between the two base alloys or between the thick $\beta+\alpha'$ layer and initial α_p grains. The bond strength is almost equal to the UTS of the Ti−22Al−25Nb base alloy. In addition, since the $\beta+\alpha'$ layer has a higher hardness and strength than the α_p grains, some cracks propagate into the α_p grains and lead to transcrystalline fracture, while most of the $\beta+\alpha'$ layers remain intact. In contrast, most of the α/α_2 layers adjacent to the interface do not crack and firmly adhere to the interface because they are refined into small grains due to the recrystallization; thus, they have a higher strength and toughness than the coarse α_p grains.

The tensile fracture morphologies of the base alloys, Ti−6Al−4V and Ti−22Al−25Nb, are shown in Figs. 9(a, b), and the deep dimples imply that they both undergo typical ductile fracture. Figures 9(c, d) show the fracture morphologies of the Ti−6Al−4V and Ti−22Al−25Nb sides of the joint, which are different from those of the two base alloys and also different from each other. The fracture surfaces on both sides are composed of two typical regions, which are marked with “A” and “B”. Region A on both sides displays a relatively flat surface and occupies most of the surface area, which should undergo brittle fracture along the bonding interface. Region B on the Ti−6Al−4V side is composed of a moderate number of irregularly-shaped cavities, which correspond to Region BI in Fig. 8(a). In contrast, in Region B on Ti−22Al−25Nb

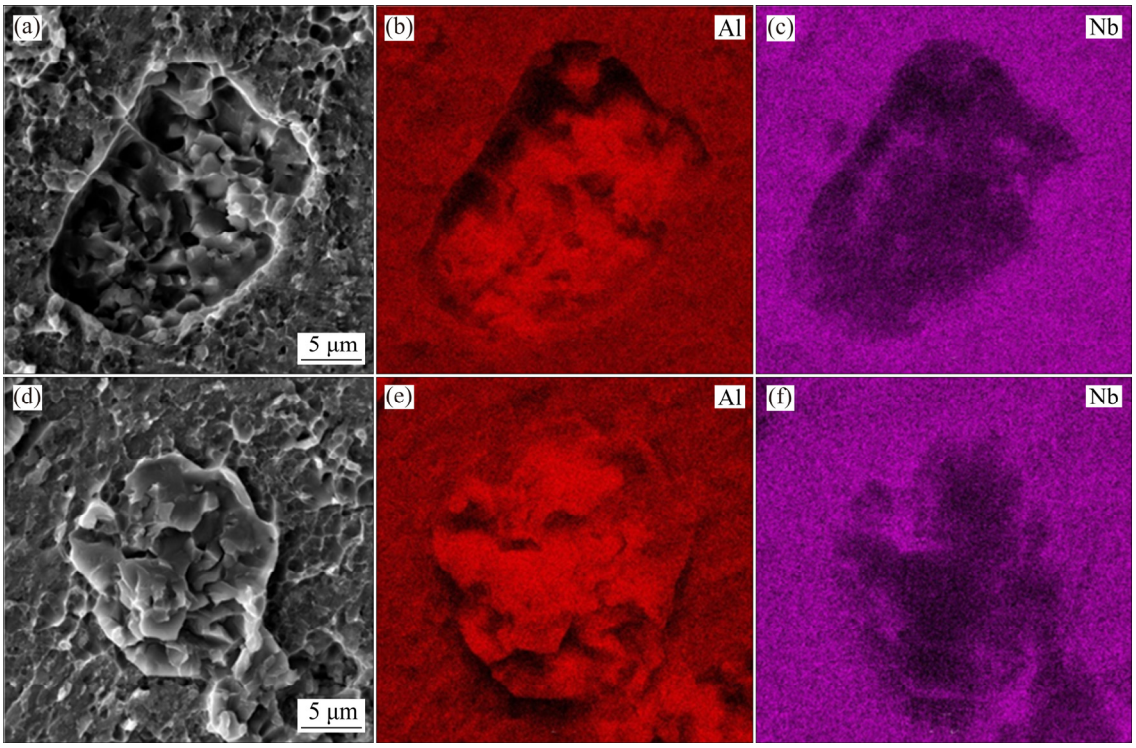

Fig. 10 SEM images and EDS maps showing distributions of Al and Nb for joint fracture morphology: (a, b, c) On Ti−6Al−4V side; (d, e, f) On Ti−22Al−25Nb side

side, there are just as many irregularly-shaped bulges as there are cavities on Ti−6Al−4V side, which corresponds to Region BII in Fig. 8(a). This implies reciprocal causation of the cavities and bulges, and both result from the fracture along the boundaries between the $\beta+\alpha'$ layers and primary α_p grains or from the transcrystalline fracture of α_p grains.

Figure 10 shows the EDS maps describing the qualitative distribution of Al and Nb on both sides of the fractured joint. Both the cavities on the Ti−6Al−4V side and the bulges on the Ti−22Al−25Nb side are rich in Al and poor in Nb, further proving that the fracture in these regions occurs in the primary α_p grains.

4 Conclusions

(1) An obvious diffusion layer forms around the interface between the two base alloys, which can be divided into two sub-layers. A discontinuous α/α_2 phase layer is formed adjacent to the interface, and a necklace-shaped $\beta+\alpha'$ martensitic structure layer is formed between the interface and Ti−6Al−4V base alloy.

(2) Downhill diffusion for all elements occurs across the interface. Nb and Al atoms mainly diffuse from the Ti−22Al−25Nb side into the β and α phases on the Ti−6Al−4V side, respectively. A few V atoms on the Ti−6Al−4V side diffuse into the *B*2 phase on the Ti−22Al−25Nb side. In the diffusion layer, the content of any element at a given point mainly depends on the distance of this point from the interface and the phase type where the point is located. The diffusion occurs in both the transverse and longitudinal directions.

(3) The Vickers microhardness of the $\beta+\alpha'$ diffusion layer on the Ti−6Al−4V side is HV 385, which is higher than that of the α_p grain (HV 347) and $\beta+\alpha_s$ colony structure (HV 308) due to the precipitation strengthening effect of acicular martensitic α'-phase and the solution strengthening effect of Al and Nb atoms. The hardness of the *B*2 layer decreases from HV 324 to HV 309 in the Ti−22Al−25Nb base alloy because Al and Nb atoms diffuse from the *B*2 layer on the Ti−22Al−25Nb side and the *O*-phase precipitates dissolve, which weakens the solution strengthening and precipitation strengthening effects, respectively.

(4) Deformation mainly occurs on the Ti−22Al−25Nb side due to its lower YS than Ti−6Al−4V. The tensile strength of the joint is

894 MPa, which is nearly equal to the UTS of the Ti−22Al−25Nb base alloy. The fracture surfaces on both sides of the joint are composed of two typical regions. One region fractures along the bonding interface via brittle fracture. The other results from fracture along the boundaries between $\beta+\alpha'$ layers and primary α_p grains or from the transcrystalline fracture of α_p grains.

Acknowledgments

The authors are grateful for the financial supports from the National Natural Science Foundation of China (No. 51505323), and State Key Laboratory of Advanced Welding and Joining, Harbin Institute of Technology, China (No. AWJ-17M-04).

References

[1] WRONSKI M, KUMAR M A, CAPOLUNGO L, MCCABE R J, WIERZBANOWSKI K, TOME C N. Deformation behavior of CP-titanium: Experiment and crystal plasticity modeling [J]. Materials Science & Engineering A, 2018, 724: 289−297.

[2] NARAYANA P L, KIM S W, HONG J K, REDDY N S, YEOM J T. Tensile properties of a newly developed high-temperature titanium alloy at room temperature and 650 °C [J]. Materials Science & Engineering A, 2018, 718: 287−291.

[3] NANDY T K, BANERJEE D. Creep of the orthorhombic phase based on the intermetallic Ti_2AlNb [J]. Intermetallics, 2000, 8: 915−928.

[4] SAROSI P M, HRILJAC J A, JONES I P. Atom location by channelling-enhanced microanalysis and the ordering of Ti_2AlNb [J]. Philosophical Magazine, 2003, 83(35): 4031−4044.

[5] KUNPFERT J. Intermetallic alloys based on orthorhombic titanium aluminide [J]. Advanced Engineering Materials, 2001, 3(11): 851−864.

[6] ÇAM G, KOÇAK M. Progress in joining of advanced materials [J]. International Materials Reviews, 1998, 43(1): 1−44.

[7] ÇAM G, KOÇAK M. Progress in joining of advanced materials−Part I: Solid state joining, fusion joining, and joining of intermetallics [J]. Science and Technology of Welding and Joining, 1998, 3(3): 105−126.

[8] ELREFAEY A, TILLMANN W. Solid state diffusion bonding of titanium to steel using a copper base alloy as interlayer [J]. Journal of Materials Processing Technology, 2009, 209(5): 2746−2752.

[9] ÇAM G, CLEMENS H, GERLING R, KOÇAK M. Diffusion bonding of fine grained gamma TiAl sheets [J]. Z Metallkd, 1999, 90(4): 284−288.

[10] ÇAM G, BOHM K H, MÜLLAUER J, KOÇAK M. The fracture behavior of diffusion-bonded duplex gamma TiAl [J]. The Journal of the Minerals, Metals and Materials Society, 1996, 48(11): 66−68.

[11] ÇAM G, MÜLLAUER J, KOÇAK M. Diffusion bonding of two-phase gamma TiAl alloys with duplex microstructure [J]. Science and Technology of Welding and Joining, 1997, 2(5): 213−219.

[12] NAEIMIAN H, MOFID M A. TLP bonding of Ti−6Al−4V to Al 2024 using thermal spray Babbitt alloy interlayer [J]. Transactions of Nonferrous Metals Society of China, 2020, 30(5): 1267−1276.

[13] ÇAM G, IPEKOĞLU G, BOHM K H, KOÇAK M. Investigation into the microstructure and mechanical properties of diffusion bonded TiAl alloys [J]. Journal of Materials Science, 2006, 41(16): 5273−5282.

[14] DENG Y H, GUAN Q, TAO J. Effect of heating time on bonding interface, atom diffusion and mechanical properties of dissimilar titanium joints produced by thermal self-compressing bonding [J]. Transactions of Nonferrous Metals Society of China, 2018, 28(4): 662−668.

[15] ÇAM G, KOÇAK M. Diffusion bonding of investment cast gamma TiAl [J]. Journal of Materials Science, 1999, 34(14): 3345−3354.

[16] ÇAM G, CLEMENS H, GERLING R, KOÇAK M. Diffusion bonding of gamma TiAl sheets [J]. Intermetallics, 1999, 7(9): 1025−1031.

[17] HOLMQUIST M, RECINA V, OCKBORN J, PETTERSSON B, ZUMALDE E. Hot isostatic diffusion bonding of titanium alloy Ti−6Al−4V to gamma titanium aluminide IHI alloy 01A [J]. Scripta Materialia, 1998, 39(8): 1101−1106.

[18] HOLMQUIST M, RECINA V, PETTERSSON B. Tensile and creep properties of diffusion bonded titanium alloy IMI 834 to gamma titanium aluminide IHI alloy 01A [J]. Acta Materialia, 1999, 47(6): 1791−1799.

[19] WANG X R, YANG Y Q, LUO X, ZHANG W, ZHAO G M, HUANG B. An investigation of Ti−43Al−9V/Ti−6Al−4V interface by diffusion bonding [J]. Intermetallics, 2013, 36: 127−132.

[20] LI Hong, YANG Chao, SUN Li-xing, LI Miao-quan. Influence of pressure on interfacial microstructure evolution and atomic diffusion in the hot-press bonding of Ti−33Al−3V to TC17 [J]. Journal of Alloys and Compounds, 2017, 720: 131−138.

[21] XUE Z, YANG Q, GU L, HAO X, REN Y, GENG Y. Diffusion bonding of TiAl based alloy to Ti−6Al−4V alloy using amorphous interlayer [J]. Materialwissenschaft und Werkstofftechnik, 2015, 46(1): 40−46.

[22] ELSHAER R N, IBRAHIM K M. Effect of cold deformation and heat treatment on microstructure and mechanical properties of TC21 Ti alloy [J]. Transactions of Nonferrous Metals Society of China, 2020, 30(5): 1290−1299.

[23] CHEN Kui-wai, PAN Su-ping, LIU Hui-qun, JIANG Yong. Effect of α phase morphology on fatigue crack growth behavior of Ti−5Al−5Mo−5V−1Cr−1Fe alloy [J]. Transactions of Nonferrous Metals Society of China, 2020, 30(9): 2459−2471.

[24] ZAFARI A, XIA K. Stress induced martensitic transformation in metastable β Ti−5Al−5Mo−5V−3Cr alloy: Triggering stress and interaction with deformation bands [J]. Materials Science & Engineering A, 2018, 724: 75−79.

[25] EISENBARTH E, VELTEN D, MÜLLER M, THULL R,

BREME J. Biocompatibility of β-stabilizing elements of titanium alloys [J]. Biomaterials, 2004, 25(26): 5705−5713.

[26] ELIAS L M, SCHNEIDER S G, SCHNEIDER S, SILVA H M, MALVISI F. Microstructural and mechanical characterization of biomedical Ti–Nb–Zr(–Ta) alloys [J]. Materials Science & Engineering A, 2006, 432(1−2): 108−112.

[27] YAN C, TILAK B, MYEONG-HEOM P. Factors determining room temperature mechanical properties of bimodal microstructures in Ti−6Al−4V alloy [J]. Materials Science & Engineering A, 2018, 730: 217−222.

[28] LÜTJERING G. Influence of processing on microstructure and mechanical properties of (α+β) titanium alloys [J]. Materials Science & Engineering A, 1998, 243(1−2): 32−45.

[29] JUN T S, SERNICOLA G, DUNNE F P E, BRITTON T B. Local deformation mechanisms of two-phase Ti alloy [J]. Materials Science and Engineering A, 2016, 649: 39−47.

[30] BOEHLERT C J. Part III. The tensile behavior of Ti−Al−Nb *O*+Bcc orthorhombic alloys [J]. Metallurgical & Materials Transactions A, 2001, 32(8): 1977−1988.

Ti−6Al−4V/Ti−22Al−25Nb 扩散连接接头的显微组织和力学性能

林 鹏[1,2]，席先铮[1]，赵文凯[1]，杨蕊红[1]，林 飞[1]，崔晓磊[2]，刘 钢[2]

1. 太原理工大学 材料科学与工程学院，太原 030024；
2. 哈尔滨工业大学 先进焊接与连接国家重点实验室，哈尔滨 150001

摘 要：在 950 °C、15 MPa 和 100 min 条件下对 Ti−6Al−4V (质量分数，%)和 Ti−22Al−25Nb (摩尔分数，%)合金进行扩散连接，并对接头的显微组织和力学性能进行研究。扩散层由 *B*2 相层、α/α_2 相层和项链状的 β+α'相层组成。扩散层某一点的成分取决于该点到界面的距离和该点所处的相的类型。接头的抗拉强度为 894 MPa，和 Ti−22Al−25Nb 基体的强度相当。接头断面由两类区域组成：一类区域为相对较平的断面，沿界面发生断裂；另一类为 Ti−6Al−4V 端形状不规则的空洞和 Ti−22Al−25Nb 端形状不规则的凸起。这两类区域均为沿 β+α'相层和 α_p 相晶粒的界面断裂或为 α_p 相晶粒的穿晶断裂。

关键词：扩散连接；Ti−6Al−4V；Ti−22Al−25Nb；界面；扩散层

(Edited by Bing YANG)